Condition Monitoring of Wind Turbine Anemometers Based on Combined Model Deep Learning

Anfeng Zhu, Qiancheng Zhao(✉), Tianlong Yang, and Ling Zhou

Engineering Research Center of Hunan Province for the Mining and Utilization of Wind Turbines Operation Data, Hunan University of Science and Technology, Xiangtan 411201, China
hnustzaf@mail.hnust.edu.cn

Abstract. The dynamic working environment brings challenges to the condition monitoring of anemometers. To accurately grasp the actual performance status of wind turbines (WTs) and timely detect anemometer faults, a combination of Particle Swarm Optimization (PSO) and the long and short term memory network (LSTM) based anemometer status monitoring method is proposed. Firstly, utilizing the wind speed data collected by the anemometer as an input variable, select the wind turbine (WT) with high similarity through similarity analysis. Then, use the PSO to enhance the structural parameters of the LSTM network to acquire efficient anemometer state estimation. This method can monitor the abnormal state of the anemometer and reconstruct the faulty wind speed data. Finally, to demonstrate the efficiency of the approach, the condition of the WT anemometer is predicted using examples.

Keywords: Wind turbine · Anemometer · Deep learning networks · Condition monitoring

1 Introduction

Due to the growth of industrialization, the dilemma of petrochemical energy is becoming increasingly apparent. As an environmentally friendly and economical green energy, wind energy has great development potential [1]. Over the past few years, WT assembly capacity has continued to grow both onshore and offshore. However, as a large and complex electromechanical equipment, WTs are generally located in remote areas and operate in harsh environments [2]. Most components of WTs, such as generators, bearings, and anemometers, are prone to failures, with electrical system components having the highest frequency of failure, followed by sensors [3]. Therefore, it is necessary to monitor the status of WT sensors, which helps to increase improving the economic benefits of the wind power industry [4, 14].

The monitoring system for WTs includes anemometers, wind vanes, voltage sensors, and current sensors. Over 40% of WT failures are caused by sensor related system failures [3–5]. A sensor failure may result in the control mechanism to issue incorrect

H. Lu and J. Cai (Eds.): ISAIR 2023, CCIS 1998, pp. 76–85, 2024.
https://doi.org/10.1007/978-981-99-9109-9_8

control instructions, which will directly affect the safety of WTs and personnel [6]. As a result, it is crucial to monitor the condition of the anemometer. Domestic and foreign scholars have made many research achievements involving fault detection and status monitoring of WT sensors. In reference [7, 15], a condition monitoring approach of temperature sensor of the main bearing and generator based on deep learning is proposed. In reference [8] used a novel auto associative neural network for fault diagnosis of WT anemometers. In reference [9] condition monitoring of WT gearbox gear based on SCADA data using cascaded and bidirectional deep learning approach is proposed. In reference [10], a condition monitoring method based on classifier fusion is recommended to extract characteristics from the observed dates, which improves the accuracy of fault detection.

However, these methods do not account for the relationship between sensors and how that relationship affects WTs. Therefore, a state monitoring method for WT anemometers based on deep learning is proposed. Aiming at the problem that it is difficult to reasonably select LSTM network parameters, PSO is used to improve the model parameters. This method can monitor the abnormal state of the anemometer and reconstruct the faulty wind speed data. Finally, the examples are used to predict the state of the WT anemometer, verifying the effectiveness of this approach. It can realize the status monitoring of the anemometer.

2 Methodology

2.1 Correlation

Correlation analysis is the analysis of the relevant factors of two or more variables, thereby determining the degree of correlation between variable factors. Highly connected variables are those with a correlation coefficient higher than 0.8. The Pearson correlation coefficient is calculated as follows:

$$r = \frac{\sum_{i=1}^{n} (X_i - \overline{X})(Y_i - \overline{Y})}{\sqrt{\sum_{i=1}^{n} (X_i - \overline{X})^2} \sqrt{\sum_{i=1}^{n} (Y_i - \overline{Y})^2}} \tag{1}$$

where $\overline{X}$ represents X average value, $\overline{Y}$ indicates Y average value, n is the number of samples.

2.2 Particle Swarm Optimization

The PSO is commonly employed to enhance each hyperparameter of a neural network to obtain the parameter combination with the highest accuracy of the neural network. The purpose of this approach is designed to simulate the behavioral characteristics of animal foraging behavior in nature. Compared to random search algorithms such as grid search and genetic algorithm, PSO has better performance [11, 13].

Establish a particle group $X = \{x_1, x_2, \cdots, x_m\}$ with a scale of m, in which a particle can be represented as a coordinate $x_i = (x_{i1}, x_{i2}, \cdots, x_{im})^T$ in the D-dimensional space,

the velocity of the particle can be written as $v_i = (v_{i1}, v_{i2}, \cdots, v_{im})^T$, and the fitness function is $f(X_i)$. During the calculation iteration process, the localized best solution of a single particle and the global best solution of the entire society will be saved, and the position and velocity of each particle will always be refreshed during this process. The updated equation is:

$$V_{id}^{k+1} = \omega V_{id}^{k} + c_1 r_1 \left(P_{id}^{k} - X_{id}^{k}\right) + c_2 r_2 \left(P_{gd}^{k} - X_{id}^{k}\right) \tag{2}$$

$$X_{id}^{k+1} = X_{id}^{k} - V_{id}^{k+1} \tag{3}$$

where $d = 1, 2, 3 \cdots, n, \quad i = 1, 2, \cdots, m$, that is, there are m particle elements in the particle swarm, k represents the iteration number of particles, c_1 and c_2 is the acceleration factor, and P_{gd}, P_{id} are the global and self optimal solutions of the particle.

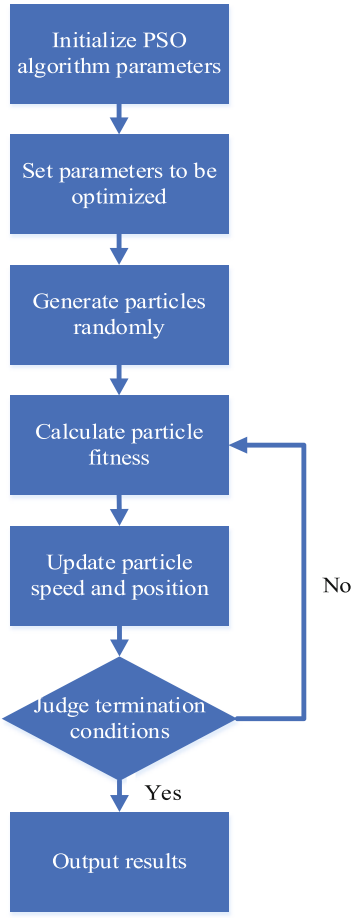

Fig. 1. Particle swarm optimization algorithm flowchart.

Figure 1 shows the workflow of the PSO. The following are the steps to apply the PSO:

(1) Set the PSO algorithm parameters, including inertia weight, acceleration factor, and population size.
(2) The dimension of the population particles is determined based on the parameters to be optimized in the neural network prediction approach. These parameters to be optimized are the optimization objectives of the particle swarm optimization algorithm. At the same time, it is necessary to determine the value range of these parameters, and randomly generate particle positions within the value range.
(3) Set the fitness function, input the parameters to be optimized into the PSO algorithm, and set the initialization value. Input the initialization value as the optimal result into the neural network to calculate the fitness.
(4) Compare the fitness of all particles with their optimal location, and then select the optimal location as the optimal historical location.
(5) Refresh the position and velocity of particles according to formulas (2) and (3).
(6) Set the optimization goal, and stop when the goal requirements are met. If the requirements are not met, rerun Step 3. The optimization goal is usually achieved by setting a fitness threshold and a maximum number of iterations.

2.3 Long and Short Term Memory Network

LSTM is an improved version of RNN. To address the issue that RNN is not suitable for long sequence information, an LSTM additionally sets a forgetting gate to control memory transfer and update in addition to the existing input and output gates of RNN. The forgetting gate prevents the movement of pointless information from the past while

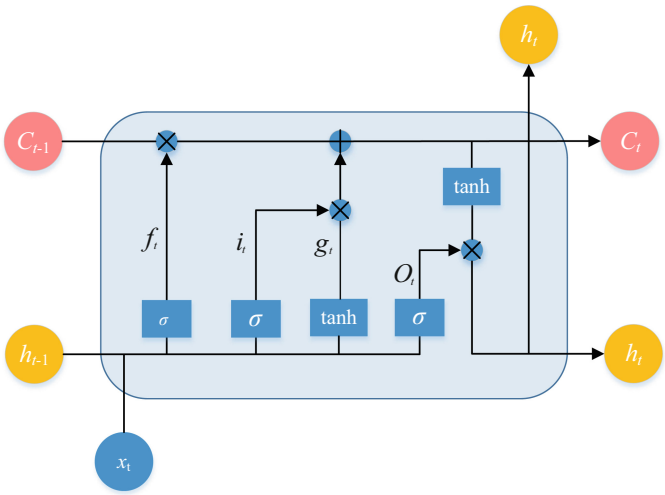

Fig. 2. Structure of LSTM.

preserving useful information. This measure optimizes RNN's performance for long-term memory, Optimized the performance of the algorithm [12]. Figure 2 depicts the construction of the LSTM.

3 Experimental Settings

3.1 Data Preparation

The data employed in this study originated from a wind farm in southern China. To confirm the predictive capability of the proposed approach, the data utilized is from the No. 7 WT in June 2015, with a data sampling time of 10 min. The data includes 2000 samples, the 1–1600 samples for training, and the 1601–2000 samples for testing. Figure 3 displays the time series for wind speed.

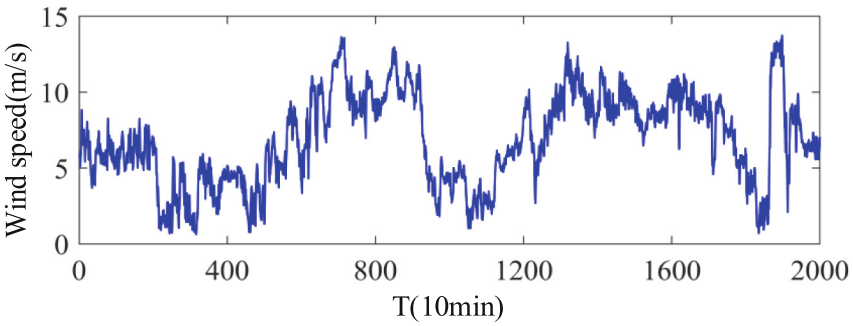

Fig. 3. Wind speed time series.

3.2 Evaluation Indicators

The modelling accuracy is evaluated applying mean absolute error (MAE), root mean square error (RMSE) and mean absolute percentage error (MAPE) indicators, and the calculation formula is:

$$\mathrm{MAE} = \frac{1}{n}\sum_{i=1}^{n}\left|\widehat{y}_i - y_i\right| \tag{4}$$

$$\mathrm{RMSE} = \sqrt{\frac{1}{n}\sum_{i=1}^{n}\left(\widehat{y}_i - y_i\right)^2} \tag{5}$$

$$\mathrm{MAPE} = \frac{1}{n}\sum_{i=1}^{n}\left|\frac{\widehat{y}_i - y_i}{y_i}\right| \tag{6}$$

where y_i is the real value; $\widehat{y}_i$ is the predicted value.

3.3 Model Structure

This study suggests a state monitoring approach for anemometers based on PSO-LSTM. Firstly, the wind speed data collected by the anemometer is employed as an input variable to select WTs with strong similarity by similarity analysis. Then, using the normal historical data of similar WTs as input data, PSO is employed to improve the parameters of the LSTM structure to enhance the state estimation of the anemometer. Finally, the prediction residual analysis is used to monitor whether the anemometer is malfunctioning, and the malfunctioning wind speed data is reconstructed. Accordingly, Fig. 4 presents the flowchart of the main contents of this study.

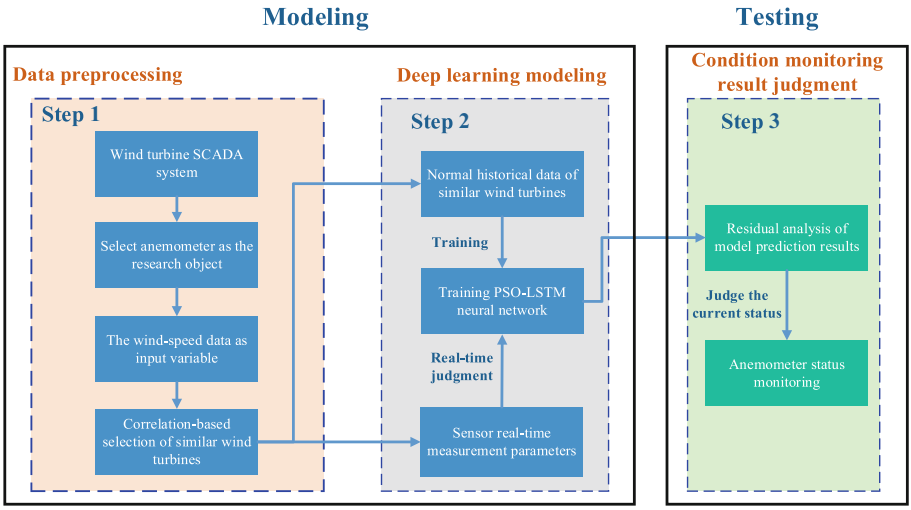

Fig. 4. Flowchart of the main contents in this study.

4 Results and Analysis

4.1 Wind Speed Correlation Analysis

Due to the complex terrain in mountainous areas, the wind speed and direction are variable, and the climate change is complex. Wind speed, as the environmental parameter that has the greatest influence on the operation of WTs, directly determines the operating status of WTs. Therefore, wind speed can be selected as a parameter to measure the similarity of the operating environment. Calculate the Pearson correlation coefficients of the wind speed series of each WT and the target WT No. 7 in the same time period. The correlation coefficients between the target WT and other WTs are shown in Table 1.

From Table 1, it can be inferred that the wind speed of the target WT No. 7 and WTs 6, 8, and 10 have extremely high correlations in wind speed data. Therefore, it is possible to choose the WT No. 7 and the WTs 6, 8, and 10 as a group of WTs with high similarity.

Table 1. Correlation between No. 7 wind turbine and others.

Wind Turbine No	Wind speed data
7	1
3	0.463
6	0.9132
8	0.9058
10	0.8906
14	0.5371
17	0.6247

4.2 Experiments Based on PSO-LSTM

Select data with normal similarity among the four WTs to train the model. According to the fault records, it can be seen that the anemometer has failed. During this period, selecting 1600 pieces of data that were previously normal as the training dataset, and 400 pieces of data that included faults as the test dataset. The final test set outcomes are exhibited in Fig. 5. Figure 5 (a) demonstrates that the model fitting effect is good and the model estimation accuracy is high. The specific residual variation is exhibited in Fig. 5 (b). It can be indicated from the graph that the residual variation is stable for most of the time, with only a few samples having significant jumps.

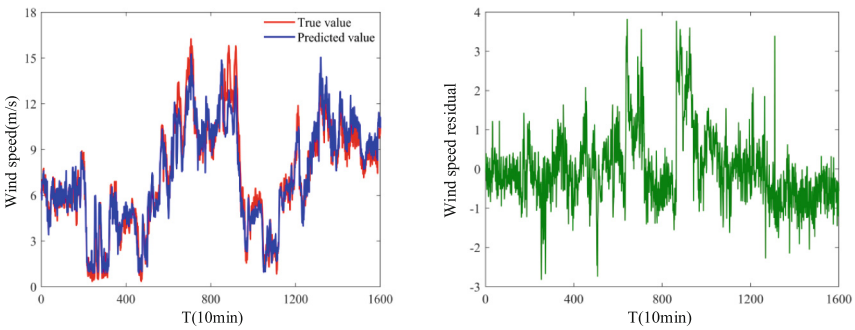

(a) Model training results (b) Model training residual

Fig. 5. Residual performance of normal data.

The PSO-LSTM model is utilized to estimate the wind speed data of the No. 7 WT that has failed. The estimated outcomes of the model are exhibited in Fig. 6 (a), and some data are abnormal due to the failure of the anemometer. The residual error is used as the basis for anomaly determination, as exhibited in Fig. 6(b). From the graph, it can be indicated that the residual error output from the 290th data point has significantly increased compared to the normal data, so it can be determined that the anemometer of No. 7 WT during this time period is in an abnormal state.

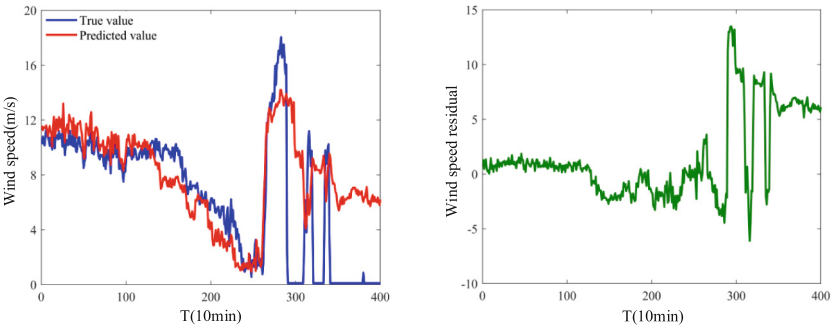

(a) Model testing results (b) Model testing residual

Fig. 6. Model test residual.

The abnormal data is reconstructed using the PSO-LSTM, as exhibited in Fig. 7. It could be found that the residual variation of the model returns to a normal range at this time. This indicates that when the anemometer is abnormal, the PSO-LSTM model is used to reconstruct the abnormal data using the similarity between WT groups. This experiment proves the effectiveness of state monitoring based on PSO-LSTM model.

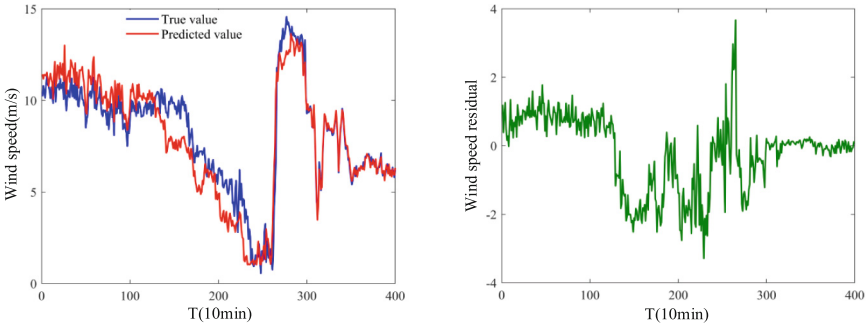

(a) Model reconstruction results (b) Model reconstruction residual

Fig. 7. Model reconstruction residual.

4.3 Comparative of Models

For further confirming the advantages of this suggested model, the reconstructed data is contrasted with the PSO-LSTM through the evaluation index of the combination Genetic Algorithm (GA) and LSTM model. The prediction results of PSO-LSTM, GA-LSTM, and LSTM are shown in Fig. 8 (a). At the same time, the assessment index of the recommended PSO-LSTM in Fig. 8(b) is greater than other approaches, so the PSO-LSTM is more precise in monitoring the operation status of the anemometer.

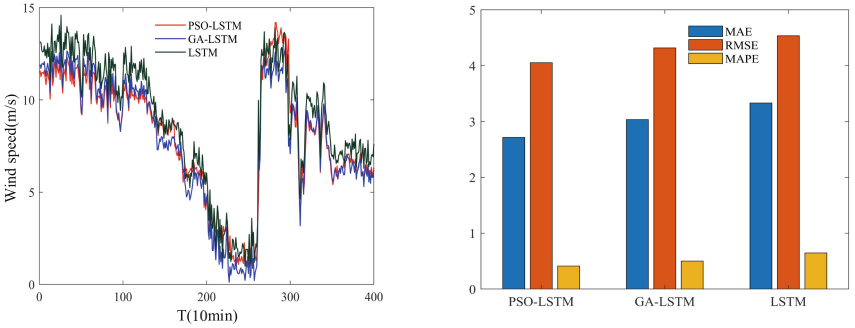

(a) Model comparison (b) Comparison of model error values

Fig. 8. Comparisons of prediction results.

5 Conclusion

Considering the dynamic working conditions of anemometer, a condition monitoring model named PSO-LSTM is suggested in this study, which is applied for condition assessment of anemometer. Using the wind speed data collected by the anemometer as input variables, select WTs with high similarity through similarity analysis. Then, take the PSO to improve the parameters of the LSTM network structure to obtain model estimates. Finally, four groups of anemometer data were analyzed to find abnormal conditions, and the abnormal wind speed data is reconstructed using the similarity between WT groups. The analysis outcomes demonstrate that the method has good accuracy, can identify abnormal states of the anemometer, and reconstruct abnormal data, improving the reliability of the anemometer.

Acknowledgments. This work is supported by National Key Research and Development Program of People's Republic of China (grant number 2022YFF0608700) and National Natural Science Foundation of China (No. 51875199).

References

1. Liu, H., Chen, C.: Data processing strategies in wind energy forecasting models and applications: a comprehensive review. Appl. Energy **249**, 392–408 (2019)
2. Zhu, A., Zhao, Q., Wang, X., et al.: Ultra-short-term wind power combined prediction based on complementary ensemble empirical mode decomposition, whale optimisation algorithm, and elman network. Energies **15**(9), 3055 (2022)
3. Pieraccini, M., Parrini, F., Fratini, M., et al.: In-service testing of wind turbine towers using a microwave sensor. Renew. Energy **33**(1), 13–21 (2008)
4. Chehouri, A., Younes, R., Ilinca, A., et al.: Review of performance optimization techniques applied to wind turbines. Appl. Energy **142**(15), 361–388 (2015)
5. Kayikci, M., Milanovic, J.V.: Reactive power control strategies for DFIG-based plants. IEEE Trans. Energy Convers. **22**, 389–396 (2007)
6. Zhu, A., Xiao, Z., Zhao, Q.: Power data preprocessing method of mountain wind farm based on POT-DBSCAN. Energy Eng. **118**(3), 549–563 (2021)

7. Fang, L., Liu, P., Zhang, B.: Sensor faults simulation of DFIG control system. Instrum. Technol. **2**, 52–54 (2014)
8. Tao, Z., Zhu, C., He, M., et al.: A physical modeling-based study on the control mechanisms of Negative Poisson's ratio anchor cable on the stratified toppling deformation of anti-inclined slopes. Int. J. Rock Mech. Min. Sci. **138**, 104632 (2021)
9. Zhu, A., Zhao, Q., Yang, T., et al.: Condition monitoring of wind turbine based on deep learning networks and kernel principal component analysis. Comput. Electr. Eng. **105**, 108538 (2023)
10. Zhou, L., Zhao, Q., Wang, X., et al.: Fault diagnosis and reconstruction of wind turbine anemometer based on RWSSA-AANN. Energies **14**(21), 6905 (2021)
11. Xiang, L., Yang, X., Hu, A., et al.: Condition monitoring and anomaly detection of wind turbine based on cascaded and bidirectional deep learning networks. Appl. Energy **305**, 117925 (2022)
12. Pashazadeh, V., Salmasi, F.R., Araabi, B.N.: Data driven sensor and actuator fault detection and isolation in wind turbine using classifier fusion. Renew. Energy **116**, 99–106 (2018)
13. Roy, C., Das, D.K.: A hybrid genetic algorithm (GA)-particle swarm optimization (PSO) algorithm for demand side management in smart grid considering wind power for cost optimization. Sādhanā **46**(2), 101 (2021)
14. Jaseena, K.U., Kovoor, B.C.: A hybrid wind speed forecasting model using stacked autoencoder and LSTM. J. Renew. Sustain. Energ. **12**(2), 023302 (2020)
15. Fu, Y., Zhang, M., Xu, X., et al.: Partial feature selection and alignment for multi-source domain adaptation. In: Proceedings of the IEEE/CVF Conference on Computer Vision and Pattern Recognition, pp. 16654–16663 (2021)
16. Kang, S., Wu, H., Yang, X., et al.: Discrete-time predictive sliding mode control for a constrained parallel micropositioning piezostage. IEEE Trans. Syst., Man Cybern. Syst. **52**(5), 3025–3036 (2021)
17. Yang, X., Wu, H., Li, Y., et al.: Dynamics and isotropic control of parallel mechanisms for vibration isolation. IEEE/ASME Trans. Mechatron. **25**(4), 2027–2034 (2020)